Thermoplasmonic-Activated Hydrogel Based Dynamic Light Attenuator

Thermoplasmonic-activated hydrogel based dynamic light attenuator

*Filippo Pierini, Alexa Guglielmelli, Olga Urbanek, Pawel Nakielski, Luigia Pezzi, Robert Buda, Massimiliano Lanzi, Tomasz A. Kowalewski and Luciano De Sio**

Dr. Filippo Pierini, Dr.Olga Urbanek, Dr. Pawel Nakielski, Prof. Tomasz A. Kowalewski
Department of Biosystems and Soft Matter and Laboratory of Polymers and Biomaterials, Institute of Fundamental Technological Research, Polish Academy of Sciences, Warsaw 02-106, Poland

Dr. Alexa Guglielmelli
Department of Physics, University of Calabria, 87036, Arcavacata di Rende, Cosenza, Italy

Dr. Alexa Guglielmelli, Dr. Luigia Pezzi, Prof. Luciano De Sio
CNR-Lab. Licryl, Institute NANOTEC, Arcavacata di Rende, 87036, Italy

Mr. Robert Buda
Institute of Physical Chemistry, Polish Academy of Sciences, ul. Kasprzaka 44/52, Warsaw 01-224, Poland

Prof. Massimiliano Lanzi
Department of Industrial Chemistry "Toso Montanari", Alma Mater Studiorum-University of Bologna, 40136 Bologna, Italy

Prof. Luciano De Sio
Center for Biophotonics and Department of Medico-Surgical Sciences and Biotechnologies, Sapienza University of Rome, Corso della Repubblica 79, 04100 Latina, Italy
E-mail: *luciano.desio@uniroma1.it*

Keywords: nanomaterials, polymers, optics, plasmonics, active plasmonics

This work describes the morphological, optical and thermo-optical properties of a temperature-sensitive hydrogel poly(N-isopropylacrylamide-*co*-N-isopropylmethacrylamide) (P(NIPAm-*co*-NIPMAm)) film containing a specific amount of gold nanorods (GNRs). The light-induced thermoplasmonic heating of GNRs is used to control the optical scattering of an initially transparent hydrogel film. A hydrated P(NIPAm-*co*-NIPMAm) film is optically clear at room temperature. When heated to temperatures over 37°C via light irradiation with a resonant source (λ=810nm) to the GNRs, a reversible phase transition from a swollen hydrated state to a shrunken dehydrated state occurs. This phenomenon causes a drastic and reversible change in the optical transparency from a clear to an opaque state. A significant red shift (≈30nm) of the

longitudinal band can also be seen due to an increased average refractive index surrounding the GNRs. This change is in agreement with an "ad-hoc" theoretical model which uses a modified Gans theory for ellipsoidal nanoparticles. Morphological analysis of the composite film shows the presence of well isolated and randomly dispersed GNRs. Thermo-optical experiments demonstrated an all-optically controlled light attenuator (65% contrast ratio) which can be easily integrated in several modern optical applications such as smart windows and light-responsive optical attenuators.

Introduction

The reduction of light intensity as it travels through a medium can be due to the reflection, absorption and/or scattering of the incident photons. The attenuation magnitude is a fundamental and important optical property that has been an important performance parameter for several technological applications ranging from optical fiber communications[1] to smart windows.[2]In recent years, polymers and liquid crystal polymer composites have been used as starting materials (instead of glass) because they offer the possibility of lightweight, cost-effective, and energy-efficient light attenuators. To this end, a lot of research interests have been focused on developing smart windows (or optical attenuators), owing to their capability of saving energy by modulating sunlight after being activated/deactivated with external stimuli such as voltage, light or heat. Depending on the nature of the external trigger, different classes of smart windows have been obtained: smart windows based on electrochromism,[3a, 3b]photochromism,[4]mechanochromism [5]and thermochromism materials.[6] Electrochromic and mechanochromic smart windows require extra devices and electricity, [7]which may bring extra energy consumption. Smart windows based on photochromism and thermochromism materials certainly represent the ideal candidates as they manage to save energy and source more efficiently.[8]Unfortunately, the photochromic materials cannot make a response under a cloudy and hot weather while the thermochromic compounds,[9]such as polymers, [10] liquid

crystals(LCs),[11a, 11b, 11c]polymer-dispersed liquid crystals (PDLCs) [12a, 12b] and vanadium dioxide (VO_2)[13] have the switching temperature much higher than environmental temperature which cause a weak change in colour/transparency. Thus, it is attractive to develop a new kind of smart switching optical devices by integrating simultaneous photo- and thermo-responsive properties. The possibility of using light instead of an electric-field is still a compelling solution because it makes it possible to develop light-sensitive optical components. Within the framework of the development of all-optical components, the driving force is represented by the possibility to use sunlight. Light-triggered optical attenuators have been based on the use of both organic (e.g. dye molecules)[14] and inorganic (e.g. metallic nanoparticles)[15] photoconverters. Plasmonic nanoparticles (NPs), such as gold and silver NPs, are excellent materials because they have an intrinsic capability to collect a large amount of visible/near infrared (NIR) light, thanks to a physical phenomenon called localized plasmonic resonance (LPR): the coherent and dipolar oscillation of the bulk free electrons localized at the metallic/dielectric interface.[16] Under a suitable frequency laser illumination associated with the LPR mechanism, the temperature significantly increases because of strong optical absorption, enabling NPs to act as a localized source of heat.[17] This remarkable property has led to a new research field called thermoplasmonics,[18] being studied in various research fields including electronics,[19] medicine,[20a, 20b] solar vapor generation[21] and catalysis.[22] The use of thermoplasmonics coupled to the control of the optical property of the NP-containing media has been studied for the last few years. By combining the photo-thermal properties of gold NPs with the thermal modulation of LCs properties, we reported on the development of dynamic Bragg mirrors,[23] Bragg attenuators,[24] diffraction gratings, and waveplates.[11c] LC-based optical components, while interesting, suffer many drawbacks such as the need to use an alignment layer or polarizers sometimes undesirable for optical attenuation application. Moreover, the production of LC-based large-area optical devices is always challenging. Temperature-responsive hydrogels have been used extensively in recent years for numerous

bio-based applications. Among them, poly(N-isopropylacrylamide-*co*-N-isopropylmethacrylamide) (P(NIPAm-*co*-NIPMAm)is a water-based, temperature-sensitive material which has been used for drug-release experiments[25] due to its capacity to become hydrophobic from hydrophilic above a critical temperature (≈ 37°C).[25, 26a, 26b, 26c] The subsequent release of water induces a drastic change in the optical transparency (from clear to opaque) of thin films. Moreover, differently from other classes of hydrogels, the hydrogel family based on poly (N-isopropylacrylamide), like P(NIPAm-*co*-NIPMAm), is well known for its chemical and structural stability even at elevated temperatures, thus exhibiting a very long shelf life.[27]For these reasons, there are several efforts devoted to improving the very low degradability of these materials in order to be more useful for biomedical applications, where the biodegradability is a mandatory requirement.[28]On the other hand, P(NIPAm-*co*-NIPMAm)-based materials have found applications in other research fields where robustness and mechanical stability are required such as optics,[29a, 29b] solar energy,[30]electronics,[31] catalysis,[32] and sensing.[33]We report on the development and characterization of a few mm-thick, optically clear, and light-responsive film composed of gold NPs uniformly dispersed in a P(NIPAm-*co*-NIPMAm) film. This film is optically activated/deactivated by exploiting the photo-thermal properties of gold NPs, enabling the development of an efficient light-triggered and dynamic optical beam attenuator.

1. Materials and method

Gold nanorods (GNRs) were selected as plasmonic NPs because they are extremely efficient photoconverters with very high photo-thermal efficiency (≈1).[34] GNRs exhibit two LPR bands (transversal and longitudinal) centered in the visible and NIR part of the electromagnetic spectrum. The longitudinal LPR band is very sensitive to the refractive index of the surrounding medium.[35a, 35b] Citrate-stabilized, water-based GNRs were synthetized using a slightly modified protocol for the seed-mediated synthesis reported in detail elsewhere.[36] **Figure 1a**

shows the absorption spectrum of the GNR solution ($C=3.2\times10^{-9}M$) with longitudinal (λ_L) and transversal (λ_T) LPR bands centered at 775 nm and 524 nm, respectively. **Figure 1b** shows the free charge distribution in an elongated NP associated with the LPR mechanism. **Figure 1c** is a representative high-resolution transmission electron microscope (TEM) image of GNRs. They are highly monodisperse with an average aspect ratio of around 3.6. A hydrogel(poly(N-isopropylacrylamide-*co*-N-isopropylmethacrylamide) (P(NIPAm-*co*-NIPMAm)))made of 95 wt% water and 5wt% of polymer was used. The precursor solution (4 ml) consisted of 231.25 mg of NIPAm (Poly(N-isopropylacrylamide), from Sigma-Aldrich), 6.25 mg of NIPMAm (N-isopropylmethacrylamide, from Sigma-Aldrich), 12.5 mg of BIS (N,N'-methylene bisacrylamide, from Roth), and 50.0 mg of Irgacure 2959 UV photo-initiator (from Sigma-Aldrich). The solution, placed in a glass vial and protected from ambient light, was stirred overnight. Subsequently, 1.0 ml of the GNRs solution was added to the polymer precursor solution. In order to fabricate flat discs with an excellent optical quality, Petri dishes (WillCo-dish ®, GWSt-5030) with 30 mm diameter were treated using an oxidation plasma (by Diener Electronic GmbH-Co. KG, Zepto) for 15 min **(Figure 2a)**. The P(NIPAm-*co*-NIPMAm) /GNRs solution was deoxygenated for 10 minutes via Argon bubbling, and then 0.5 ml of solution was poured into each Petri dish **(Figure 2b)**. In order to keep the temperature below 20°C during the photopolymerization process, the Petri dishes were put into an ice bath before illuminating **(Figure 2c)** the samples from the top for 1 minute by UV light (by Dymax Europe GmbH, 5000-PC). The P(NIPAm-*co*-NIPMAm)/GNRs discs were gently detached **(Figure 2d)** from the Petri dishes and stored in water at room temperature. **Figure 2e** indicates excellent optical transparency of the sample deposited on a glass substrate (the text behind the sample can be easily read).

2. Experimental Section

The morphology of the P(NIPAm-*co*-NIPMAm)/GNRsamples **(Figure 2e)** was investigated by a field emission scanning electron microscope (FE-SEM, Nova NanoSEM 450, FEI) operating at an accelerating voltage of 10 kV. Samples were freeze-dried and coated with a 8 nm-thick gold layer prior to their characterization, in order to minimize charging. In order to study the GNRs distribution, samples were inspected by a transmission electron microscope (TEM, FEI Talos F200X - 200 kV). Samples were first freeze-dried, then the lyophilized materials were cut into small pieces, immersed in ethanol, and placed on a copper mesh with an amorphous carbon membrane. The samples were dried in a vacuum for 4h. Light-triggered experiments were conducted using the thermo-optical setup illustrated in **Figure 3**. This setup uses a CW pump laser (Coherent Inc.) operating at 810 nm (within the LPR of these GNRs (**Figure 1a**)), a collimated white light source (CLS 100, Leica), a spectrometer (USB 2000, Ocean Optics) for monitoring both spectral response and light attenuation behavior, and a thermal camera (A655sc, FLIR) for mapping and measuring temperature changes in the sample under laser beam illumination. The P(NIPAm-*co*-NIPMAm)/GNR samples were covered with a glass slide (100 µm thick) and the gap, controlled via 50 µm glass microspheres, was infiltrated with water. The water film acts as a reservoir to keep the samples hydrated, which is a requirement for their functionality as optical components (see below for details).

3. Results

Figure 4a-b shows FE-SEM micrographs indicating a honeycomb-like architecture composed of uniformly distributed pores with an average size of a few microns. The presence of GNRs does not affect the conventional morphology of the P(NIPAm-*co*-NIPMAm) film as this morphology is similar to previously reported system without GNRs.[26a]The stability of the P(NIPAm-*co*-NIPMAm) /GNRs morphology after a prolonged storage time (up to 45 days) in water is reported in the Supplementary Materials Section 1.**Figure 4c-d** shows TEM images

indicating well dispersed and randomly aligned GNRs within the P(NIPAm-*co*-NIPMAm) matrix. No evidence of GNRs agglomeration was observed. **Figure 5** reports a thermographic study of the P(NIPAm-*co*-NIPMAm)/GNR samples. **Figure 5a** shows that there is a significant and gradual temperature increase up to 44°C upon illumination (Pump ON) at different intensity values of the pump beam (from 393mW/cm^2 to 5060 mW/cm^2) because of the photo-thermal conversion of GNRs. The sample cools back down to room temperature as soon as the pump beam is turned off (Pump OFF). The curves shown in **Figure 5a** were obtained by processing the thermal images in **Figure 5b** with a proprietary software program (FLIR Research IR Max). **Figure 5c** shows a linear correlation between the maximum temperature (obtained from the curves shown in **Figure 5a**) and the intensity of the pump laser. This linear behavior is well in agreement with the theoretical model reported in detail elsewhere.[37]Temperature values (**Figure 5c**) were obtained by measuring the temperature with the thermal-camera (see thermo-optical setup in **Figure 3**) on the surface of the glass slide (100 µm thick) covering the P(NIPAm-*co*-NIPMAm)/GNR samples. Samples are quite thin (few millimeters thick), and for this reason we are confident that the difference between the temperature of the surface and that in the bulk of the sample is less than few degrees. The additional experiments (not shown here), performed without GNRs on similar samples, did not show any significant temperature change, thus confirming the capability of GNRs to convert the incident, resonant, light into heat. In order to understand the influence of the photo-thermal heating on the spectral position of LPR bands, the spectral response of the samples was investigated. When photo-heated to temperatures above 37°C a significant red shift (≈30nm) (**Figure 6**, blue and red curves) of the longitudinal band, due to an increase in the average refractive index of the medium surrounding the GNRs (from hydrated n≈1.4 to dehydrated P(NIPAm-*co*-NIPMAm) n≈1.5), can be observed. At room temperature with the water reservoir keeping the P(NIPAm-*co*-NIPMAm)/GNRs film hydrated, the refractive index was roughly estimated as an average between the refractive index of the water (n≈1.3) and that of the P(NIPAm-*co*-

NIPMAm)/GNRs composition (n≈1.5). Upon illumination (I= 5060 mW/cm^2) a phase transition from a swollen hydrated state to a shrunken dehydrated state occurs, producing an increased refractive index (1.5 instead of 1.4). This result is in agreement with the theoretical model which uses a slightly modified Gans theory[35a] for ellipsoidal NPs (**Figure 6**, magenta and green curves). More details on the theoretical model are offered in the Supplementary Materials Section 2. It is worth pointing out that because of the low sensitivity to refractive index variations, the transversal band is red-shifted by only a few nanometers. The ability of these films to work as a dynamic attenuator was tested by probing the samples with a collimated white light source while turning the pump beam ON and OFF on the same probed area. With the pump beam OFF (**Figure 7a**) the sample is optically clear, and all the incident probe light is transmitted producing a visible white spot on the post-mountable view screen. When the pump beam is turned ON (I=5060 mW/cm^2) there is a drastic change in the optical transparency due to the scattering of the incident probe light (**Figure 7b**). The photo-thermal-induced phase transition is driven by a morphological change of the P(NIPAm-*co*-NIPMAm) film which transforms from a straight to a shrinked conformation of the chains at temperatures above 37°C. The photo-thermal-activated area of the sample is more evident in **Figures 7c** and **7d**, where the probe beam and the probe/pump beams were turned OFF, respectively. Note: the photo shown in **Figure 7d** was quickly acquired immediately after the pump beam was turned OFF. Samples show an excellent optical reversibility and start to go back to the initial (transparent) state as soon as the pump beam is turned OFF (see the Supporting Information Movie). **Figure 8a** shows the transmission dynamic response of the sample obtained by measuring the transmitted probe light intensity while turning the pump beam ON (I= 5060 mW/cm^2) and OFF. The contrast ratio (*C*) – defined as the ratio of the transmitted intensity with the pump beam OFF (**Figure 8c**) to the incident intensity with the pump beam ON (**Figure 8d**) – in percentage, is 65%. Response times (ON and OFF) are 52 s and 55 s, respectively. **Figure 8b** shows the exceptional reversible and repeatable change of the optical response of the sample induced by

a sequence of pump beam light pulses (10 cycles). Moreover, it is worth pointing out that the optical response of the P(NIPAm-*co*-NIPMAm)/GNR samples shows an excellent reversibility even after a long storage time in water. A detailed characterization is .reported in the Supplementary Materials Section 1.Transmission spectra reported in **Figure 8e** acquired by turning ON (red curve) and OFF (blue curve) the pump beam (I=5060 mW/cm^2) evidence the capability of the sample to attenuate the incident (unpolarized) probe white light in a relatively large spectral range (from 400 to 800 nm) with an average *C* of about 65%. In addition, as previously discussed (**Figure 6**), there is an evident red-shift (≈30 nm) of the longitudinal plasmon band. Noteworthy at room temperature the transmission of the sample is higher than 90%, thus confirming its extraordinary optical quality in terms of optical transparency. The spectral properties of the P(NIPAm-*co*-NIPMAm)/GNR samples are not affected by the prolonged hydration. A detailed characterization of the spectral properties of the samples for different hydration times (up to 45 days) is reported in the Supplementary Materials Section 1. In addition, in order to confirm the stability of the P(NIPAm-*co*-NIPMAm) matrix as well as the absence of GNRs reshaping after different cycles of photo-switching experiments, we have performed both wide angle X-ray scattering (WAXS) analysis and TEM characterization. Results reported in the Supplementary Materials Section 1 do not show any evident variation in the WAXS patterns as well as in TEM morphology, thus confirming that there has been no change in the structure of the P(NIPAm-*co*-NIPMAm) material and GNRs shape. In addition, a thermogravimetric analysis (TGA) reported in the Supplementary Materials Section 1 evidences the excellent thermal stability of the P(NIPAm-*co*-NIPMAm)/GNR samples up to 300 °C.

4. Discussions

In the light of light-triggered optical applications, our finding represent a very important step-forward in comparison with previously reported results on similar attempts[3a, 3b, 4, 5, 6, 7, 8]. The proposed P(NIPAm-*co*-NIPMAm)/GNRs optical attenuator offers flexibility, light

responsivity, optical transparency (OFF state), mechanical stability, long-lasting functionality, reversibility and the last but not the least does not require any electrical power. Moreover, thanks to the presence of an integrated water reservoir, we have faced one of the main issues of hydrogel-based materials. Indeed, the water layer keeps the P(NIPAm-*co*-NIPMAm) film in hydrated state (OFF state) at room temperature while it acts as a well to run out water from the film (ON state) at high temperature (44 °C), thus enabling a long-lasting functionality and reversibility. The optical properties of the proposed thermoplasmonic activated, hydrogel based, dynamic light attenuator can be further improved in terms of spectral sensitivity, attenuation and response times. This can be accomplished by exploiting a new generation of NPs such as nano-plates or metal-dielectric (GNRs encapsulated in a matrix made of titanium dioxide (TiO_2))[38] with a wider wavelength range in order to maximize the sunlight absorption (e.g. from UV to NIR). Reduction of the response times as well as required power density can be achieved by increasing the NPs concentration. To this end, we are actively working on a new generation of NPs with a chemically modified surface chemistry for improving the dispersibility in P(NIPAm-*co*-NIPMAm), hence allowing to increase the actual utilized concentrations. As such, this will be a key factor for minimizing the required light intensity for triggering the optical device from a clear to an opaque state, thus enabling the realization of a new generation of low power smart windows.

5. Conclusion

To summarize, we demonstrated the concept of a light-controlled optical beam attenuator by combining gold nanorods (GNRs) and a responsive hydrogel poly(N-isopropylacrylamide-*co*-N-isopropylmethacrylamide) (P(NIPAm-*co*-NIPMAm) material. The morphological, spectral, and thermo-optical properties of thin films were studied. The GNRs are very well dispersed in the polymer yet unaligned. The optical transparency can be modulated using light irradiation resonant to the longitudinal plasmonic resonance of the GNR. Optical contrast of approximately 65% was measured upon irradiation of 5060 mW/cm^2. A theoretical model which uses a

modified Gans theory for rod-like particles fits the experimental results very well. Response times (on and off) are symmetric and both falling within the one-minute time frame. We are actively working on a new generation of gold NPs with higher dispersibility in P(NIPAm-*co*-NIPMAm) in order to increase their concentration in the polymer film. This can allow to further reduce the pump intensity to a value suitable to activate the samples (e.g. down to 0.5 W/cm^2) making these materials very promising for solar light applications. However, we are confident that our results are already very promising for the development of a new generation of solar sunlight-triggered smart windows or on-demand optical attenuators.

Supporting Information

1) Morphological and optical stability of the samples;
2) Theoretical model based on a modified Gans theory;
3) Movie: reversible change of the transmitted intensity induced by turning the pump beam ON and OFF.

Acknowledgements

Authors are thankful to Timothy J. Bunning for the fruitful discussions. The research leading to the reported results has received funding from: Air Force Office of Scientific Research (AFOSR), Air Force Research Laboratory (AFRL) and U.S. Air Force grant number FA9550-18-1-0038 (P. I. L. De Sio, EOARD 2017-2020) and the Materials and Manufacturing Directorate, AFRL; by the National Science Centre (NCN) grant no. 2015/19/D/ST8/03196 and the National Agency for Academic Exchange (NAWA) grant no. PPI/APM/2018/1/00045/U/001. The manuscript was written through contributions of all authors. All authors have given approval to the final version of the manuscript.

Received: ((will be filled in by the editorial staff))
Revised: ((will be filled in by the editorial staff))
Published online: ((will be filled in by the editorial staff))

References

[1] L. Anping, U. Kenichi, Optics Communications 1996, 132, 511.
[2] C. G. Granqvist, Smart Materials Bulletin 2002, 2002, 9.
[3] a)G. Cai, P. Darmawan, X. Cheng, P. S. Lee, Advanced Energy Materials 2017, 7, 1602598; b)A. K. Singh, S. Kiruthika, I. Mondal, G. U. Kulkarni, Journal of Materials Chemistry C 2017, 5, 5917.
[4] L. Y. L. Wu, Q. Zhao, H. Huang, R. J. Lim, Surface and Coatings Technology 2017, 320, 601.
[5] H.-N. Kim, D. Ge, E. Lee, S. Yang, Advanced Materials 2018, 30, 1803847.
[6] J.-L. Wang, Y.-R. Lu, H.-H. Li, J.-W. Liu, S.-H. Yu, Journal of the American Chemical Society 2017, 139, 9921.
[7] R. Vergaz, J.-M. Sánchez-Pena, D. Barrios, C. Vázquez, P. Contreras-Lallana, Solar Energy Materials and Solar Cells 2008, 92, 1483.
[8] D. Cao, C. Xu, W. Lu, C. Qin, S. Cheng, Solar RRL 2018, 2, 1700219.
[9] F. Chen, Y. Ren, J. Guo, F. Yan, Chemical Communications 2017, 53, 1595.
[10] A. L. Dyer, C. R. G. Grenier, J. R. Reynolds, Advanced Functional Materials 2007, 17, 1480.
[11] a)H. Wang, L. Wang, H. Xie, C. Li, S. Guo, M. Wang, C. Zou, D. Yang, H. Yang, RSC Advances 2015, 5, 33489; b)K. M. Lee, V. P. Tondiglia, T. J. White, MRS Communications 2015, 5, 223; c)L. De Sio, P. F. Lloyd, N. V. Tabiryan, T. Placido, R. Comparelli, M. L. Curri, T. J. Bunning, ACS Applied Nano Materials 2019, 2, 3315.
[12] a)F. Ahmad, M. Jamil, Y. J. Jeon, Electronic Materials Letters 2014, 10, 679; b)S. Kumar, H. Hong, W. Choi, I. Akhtar, M. A. Rehman, Y. Seo, RSC Advances 2019, 9, 12645.
[13] F. Xu, X. Cao, H. Luo, P. Jin, Journal of Materials Chemistry C 2018, 6, 1903.
[14] J. R. Talukder, Y.-H. Lee, S.-T. Wu, Opt. Express 2019, 27, 4480.
[15] V. Liberman, M. Sworin, R. P. Kingsborough, G. P. Geurtsen, M. Rothschild, Journal of Applied Physics 2013, 113, 053107.
[16] L. M. Liz-Marzán, Materials Today 2004, 7, 26.
[17] G. Baffou, R. Quidant, Laser & Photonics Reviews 2013, 7, 171.
[18] G. Baffou, *Thermoplasmonics: Heating Metal Nanoparticles Using Light*, Cambridge University Press, Cambridge 2017.
[19] L. De Sio, T. Placido, R. Comparelli, M. Lucia Curri, M. Striccoli, N. Tabiryan, T. J. Bunning, Progress in Quantum Electronics 2015, 41, 23.
[20] a)R. Bardhan, S. Lal, A. Joshi, N. J. Halas, Accounts of Chemical Research 2011, 44, 936; b)F. Pierini, P. Nakielski, O. Urbanek, S. Pawłowska, M. Lanzi, L. De Sio, T. A. Kowalewski, Biomacromolecules 2018, 19, 4147.
[21] O. Neumann, A. S. Urban, J. Day, S. Lal, P. Nordlander, N. J. Halas, ACS Nano 2013, 7, 42.
[22] J. R. Adleman, D. A. Boyd, D. G. Goodwin, D. Psaltis, Nano Letters 2009, 9, 4417.
[23] L. De Sio, T. Placido, S. Serak, R. Comparelli, M. Tamborra, N. Tabiryan, M. L. Curri, R. Bartolino, C. Umeton, T. Bunning, Advanced Optical Materials 2013, 1, 899.
[24] L. De Sio, U. Cataldi, A. Guglielmelli, T. Bürgi, N. Tabiryan, T. J. Bunning, MRS Communications 2018, 8, 550.
[25] Y. Guan, Y. Zhang, Soft Matter 2011, 7, 6375.

[26] a)S. Jin, M. Liu, S. Chen, C. Gao, European Polymer Journal 2008, 44, 2162; b)D. H. Reneker, A. L. Yarin, Polymer 2008, 49, 2387; c)K. Matsumoto, N. Sakikawa, T. Miyata, Nature Communications 2018, 9, 2315.
[27] A. Saeed, D. M. R. Georget, A. G. Mayes, Journal of Polymer Science Part A: Polymer Chemistry 2010, 48, 5848.
[28] S. Lanzalaco, E. Armelin, Gels 2017, 3, 36.
[29] a)L. Dong, A. K. Agarwal, D. J. Beebe, H. Jiang, Nature 2006, 442, 551; b)M. Wei, M. J. Serpe, Particle & Particle Systems Characterization 2019, 36, 1800326.
[30] J. E. Cho, S. Kim, S. Son, J. Yang, M. S. Kang, S. H. Eom, S. C. Yoon, M. H. Kim, B. Kim, The Journal of Physical Chemistry C 2019, 123, 2755.
[31] Y. Shi, C. Ma, L. Peng, G. Yu, Advanced Functional Materials 2015, 25, 1219.
[32] S. Shi, L. Zhang, T. Wang, Q. Wang, Y. Gao, N. Wang, Soft Matter 2013, 9, 10966.
[33] B. Mutharani, P. Ranganathan, S.-M. Chen, D. V. S. K, Sensors and Actuators B: Chemical 2020, 304, 127232.
[34] Z. Qin, Y. Wang, J. Randrianalisoa, V. Raeesi, W. C. W. Chan, W. Lipiński, J. C. Bischof, Scientific Reports 2016, 6, 29836.
[35] a)R. Gans, Annalen der Physik 1912, 342, 881; b)J. Pérez-Juste, I. Pastoriza-Santos, L. M. Liz-Marzán, P. Mulvaney, Coordination Chemistry Reviews 2005, 249, 1870.
[36] J. G. Mehtala, D. Y. Zemlyanov, J. P. Max, N. Kadasala, S. Zhao, A. Wei, Langmuir 2014, 30, 13727.
[37] P. Keblinski, D. G. Cahill, A. Bodapati, C. R. Sullivan, T. A. Taton, Journal of Applied Physics 2006, 100, 054305.
[38] A. Truppi, F. Petronella, T. Placido, V. Margiotta, G. Lasorella, L. Giotta, C. Giannini, T. Sibillano, S. Murgolo, G. Mascolo, A. Agostiano, M. L. Curri, R. Comparelli, Applied Catalysis B: Environmental 2019, 243, 604.

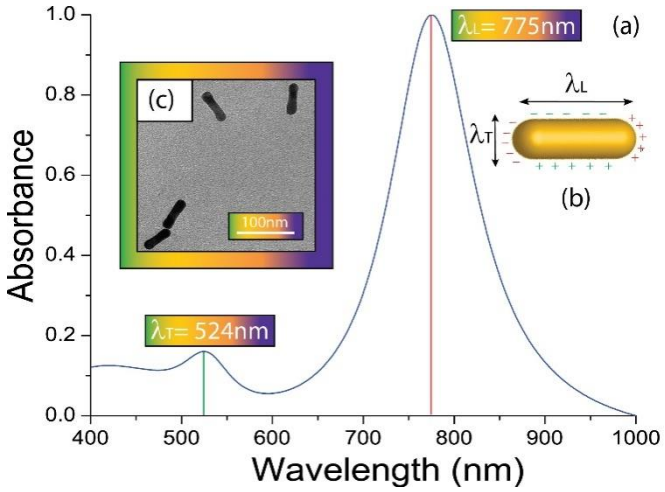

Figure 1. Absorption spectrum of a water-based GNR solution (**a**) along with a schematic representation of the LPR mechanism in a rod-like NP (**b**). High-resolution TEM image of GNRs (**c**).

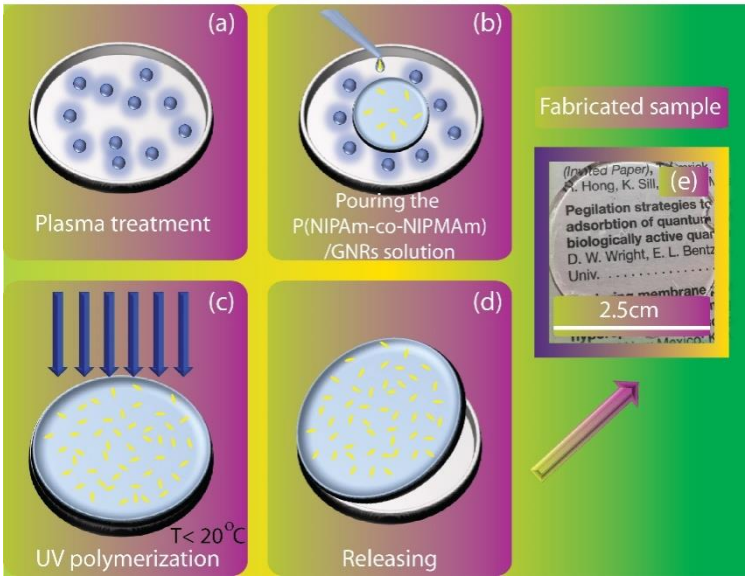

Figure 2. Step by step fabrication process of the P(NIPAm-*co*-NIPMAm)/GNRs sample.

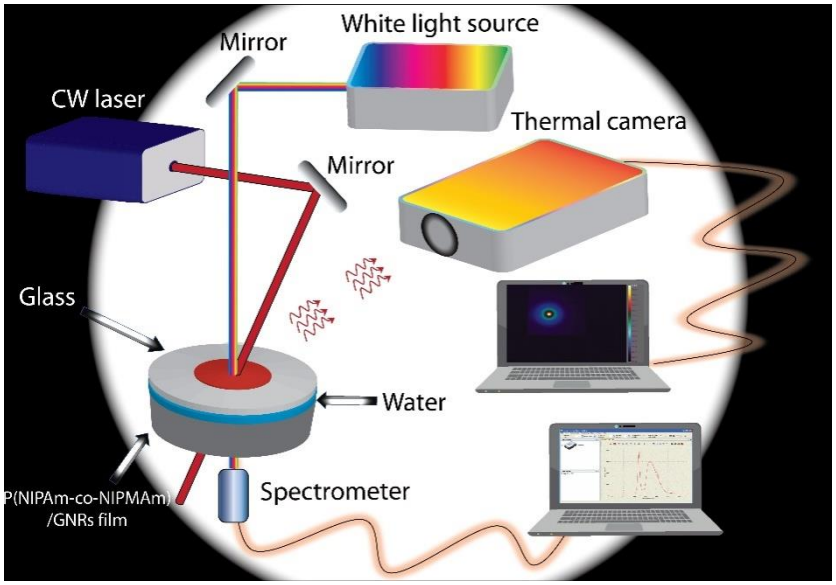

Figure 3. Thermo-optical setup for sample characterization.

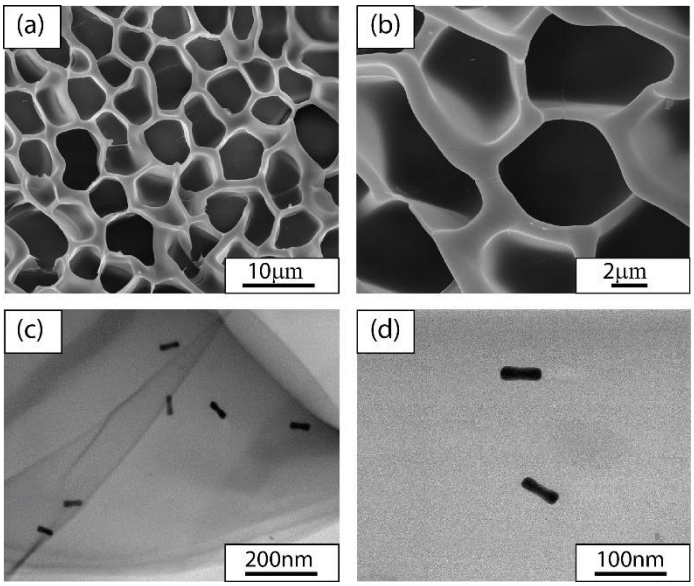

Figure 4. FE-SEM (**a**, **b**) and TEM (**c**, **d**) analysis of the P(NIPAm-*co*-NIPMAm)/GNRs sample for different magnifications.

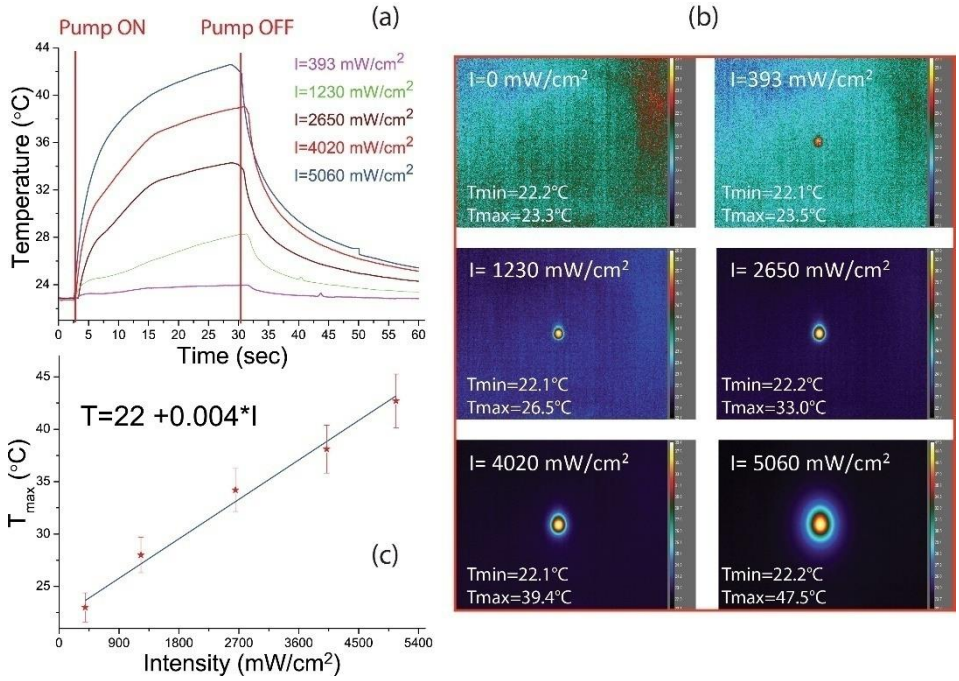

Figure 5. Time-temperature dependence of the P(NIPAm-*co*-NIPMAm)/GNRs sample under pump beam illumination (**a**) along with the corresponding thermographic view (**b**). Linear fit of the maximum temperature versus the intensity of the pump beam (**c**). T_{min} and T_{max} indicate the maximum and minimum temperature of each color scale reported in (**b**).

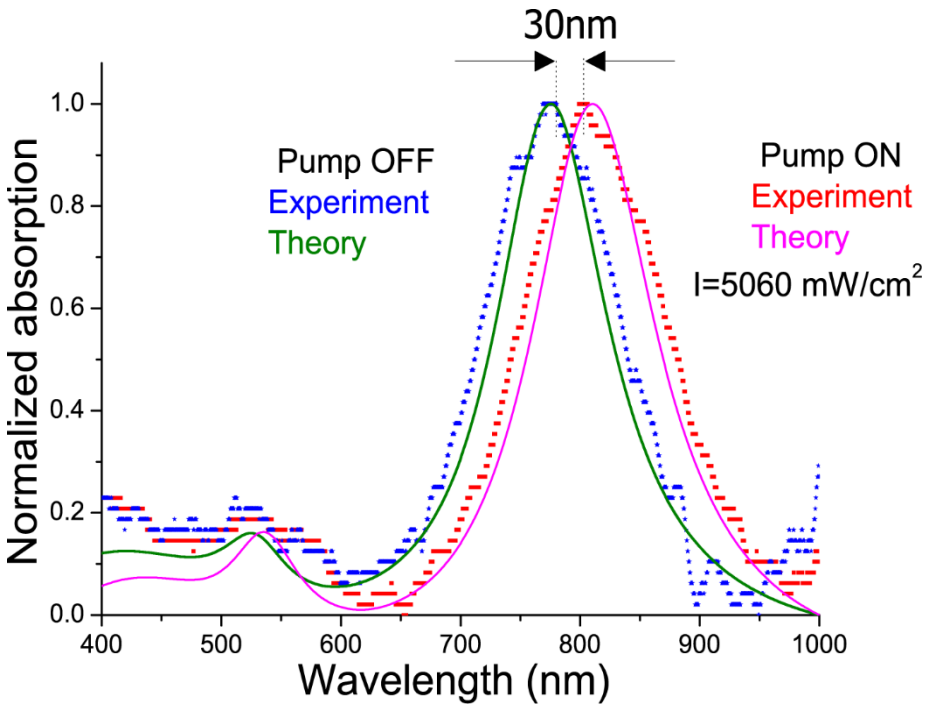

Figure 6. Theoretical (green and magenta) and experimental (blue and red) absorption spectra of the P(NIPAm-*co*-NIPMAm)/GNRs sample without (green and blue) and upon (magenta and red) pump beam irradiation.

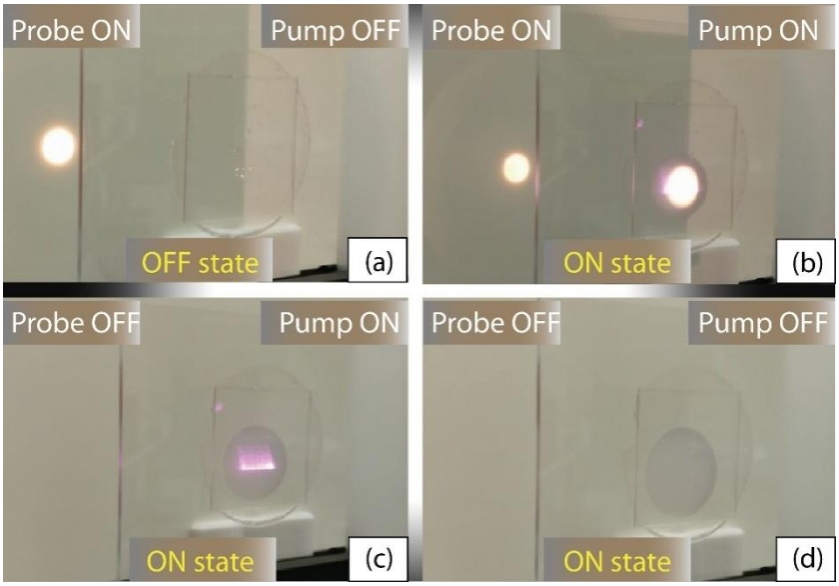

Figure 7. Photos of the P(NIPAm-*co*-NIPMAm)/GNRs sample in the OFF (**a**) and ON (**b**, **c**, **d**) states for different combinations of the probe and pump beam.

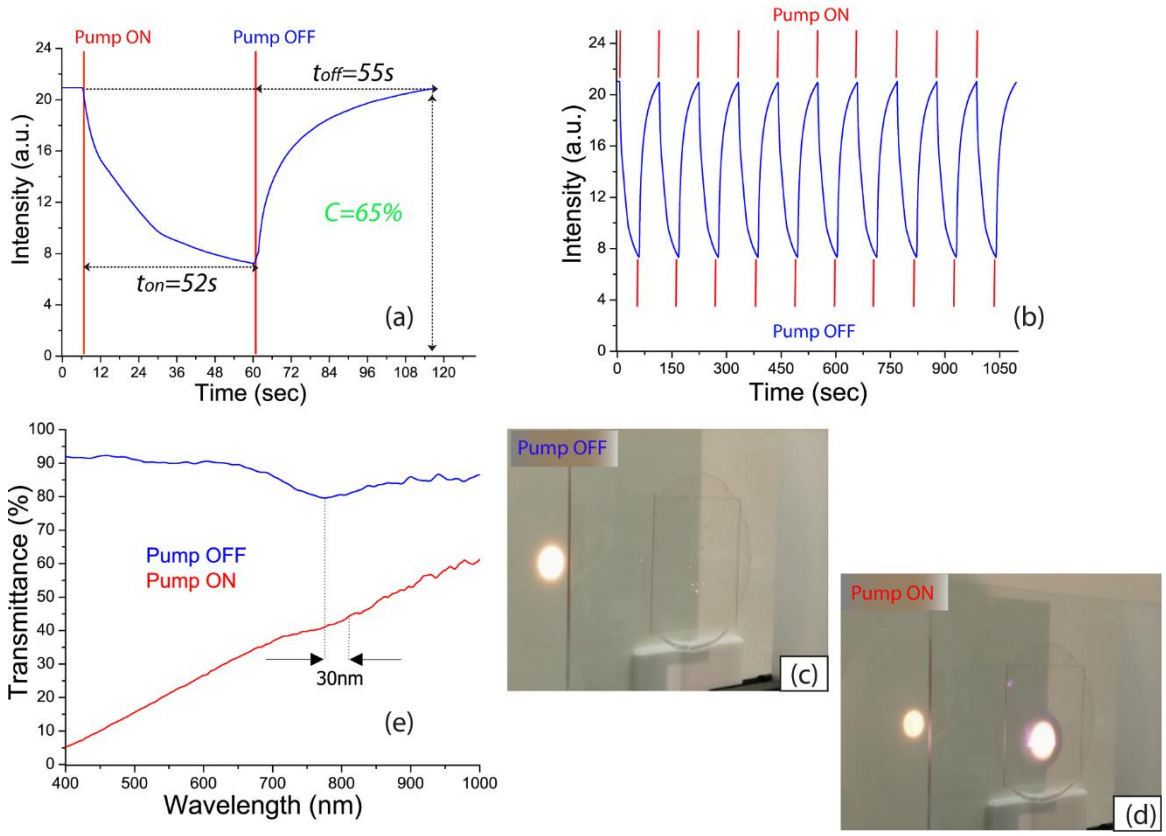

Figure 8. Reversible change of the transmitted intensity (**a,** 1 cycle),(**b**, 10 cycles) induced by turning the pump beam ON (**c**) and OFF (**d**). Transmission spectra of the sample (**e**) by turning ON (red curve) and OFF (blue curve) the pump beam.

A thermo-plasmonic activated light beam attenuator is obtained by bridging the photo-thermal properties of gold nanoparticles and the thermo-responsivity of ahydrated hydrogel film.

Keyword:nanomaterials, polymers, optics, plasmonics, active plasmonics

Filippo Pierini, Alexa Guglielmelli, Olga Urbanek, Pawel Nakielski, Luigia Pezzi, Robert Buda, Massimiliano Lanzi, Tomasz A. Kowalewski and Luciano De Sio*

Photo-thermal beam attenuator in a hydrogel film containing plasmonic nanoparticles

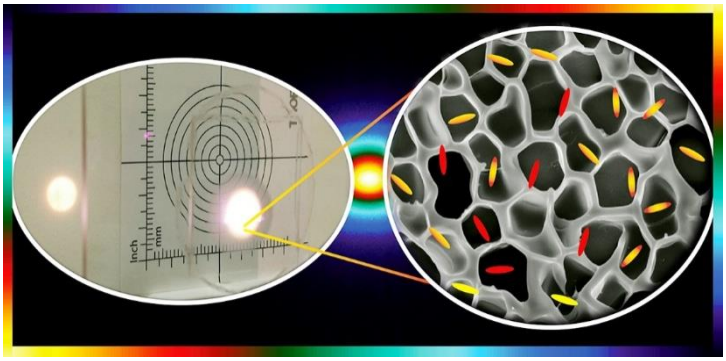

Supporting information 1

Thermoplasmonic-activated hydrogel based dynamic light attenuator

*Filippo Pierini, Alexa Guglielmelli, Olga Urbanek, Pawel Nakielski, Luigia Pezzi, Robert Buda, Massimiliano Lanzi, Tomasz A. Kowalewski and Luciano De Sio**

The stability of the P(NIPAm-*co*-NIPMAm) /GNRsamples after a prolonged storage time in water was verified by performing a detailed characterization of the morphological and optical properties. Four identical samples (see Materials and methods for technical details) were fully immersed in distilled water and investigated at t= 0 days, t= 1 day, t= 30 days, t= 45 days by a: i) field emission scanning electron microscope (FE-SEM); ii) UV-Vis spectrophotometer; iii) pump-probe optical setup. More details on these techniques are reported in the Experimental section.

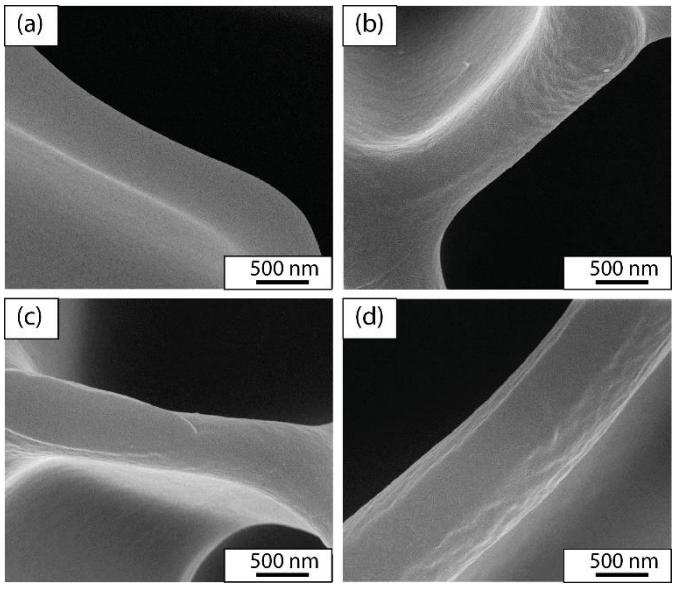

Figure S1. FE-SEM analysis of the samples at different hydration times: t= 0 days (**a**), t=1 day (**b**), t=30 days (**c**), t=45 days (**d**).

Figure **S-1(a-d)** clearly shows that the prolonged immersion in water does not affect the morphology of the P(NIPAm-*co*-NIPMAm) film. Indeed, no presence of structural defects is visible at this level of magnification, thus highlighting the extraordinary capability of theP(NIPAm-*co*-NIPMAm) material to retain its morphological properties even after 45 days of continuous hydration.

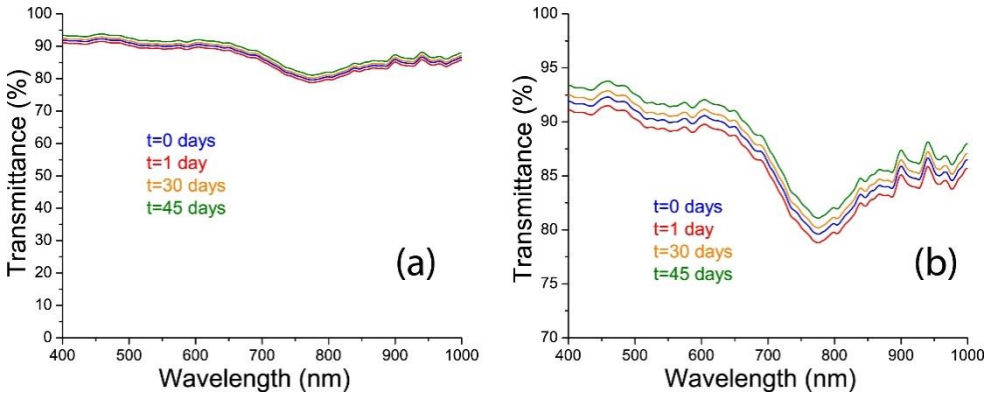

Figure S2. Spectral response of the samples at different hydration times (**a**) along with a detailed view of the same graph (**b**).

The spectral response (**Figure S-2a**) confirms that the transmission properties of the samples are not affected by the prolonged hydration. As such, the change in the transmittance is less than 2-3% (**Figure S-2a**) and this small change can be ascribed to the intrinsic experimental error of the utilized optical setup. This result clearly evidences that there is no evidence of critical instability of P(NIPAm-*co*-NIPMAm) material after prolonged storage times in water.

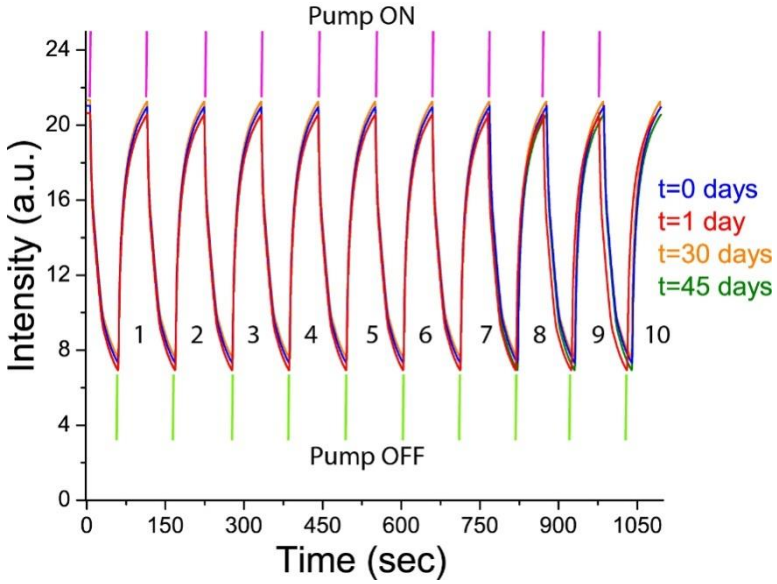

Figure S3. Reversible change of the transmitted intensity of the samples induced by cycling (from 0 to 10) the pump beam ON and OFF.

Photo-switching experiments (by cycling the sample up to 10 times)at each hydration time were conducted using the all-optical setup described in the Experimental Section. Figure **S3** shows an excellent reversibility of the transmitted intensity and no change in the optical properties in terms of response times and optical contrast is observed for all the investigated samples. It is worth pointing out that the small offset between the four curves reported in Figure **S3** can be attributed to the experimental difficulty to set the same initial intensity value for each measurement.

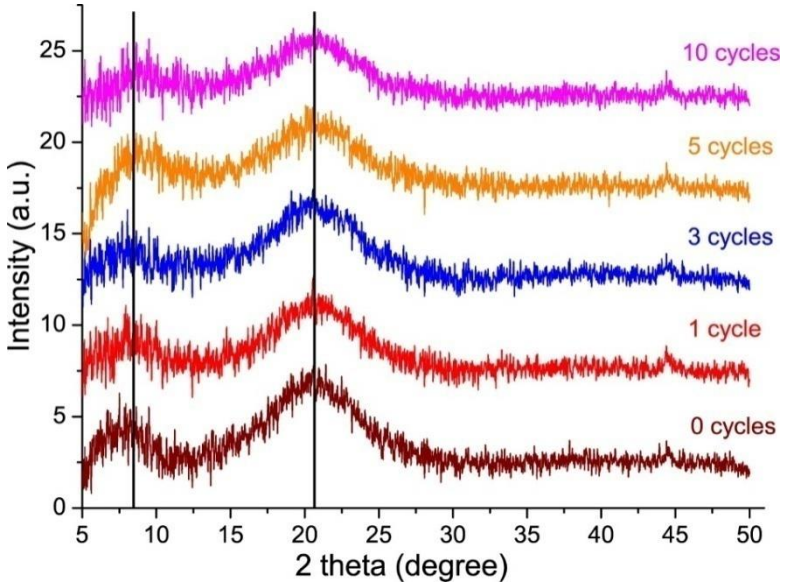

Figure S4. Wide angle X-ray scattering (WAXS) analysis of the of the samples at different cycles of photo-switching experiments.

In order to investigate the chemical structure of the P(NIPAm-*co*-NIPMAm) material and detect any potential change in matrix structure after different irradiation cycles, wide angle X-ray scattering (WAXS) analysis was performed by means of a Bruker D8 Discover diffractometer. Measurements were carried out in reflection mode, using Bragg-Brentano geometry in the angular range (2 theta) between 5 and 50 degrees, with a step of 0.02 degrees. The time of data accumulation at a particular angular point was 1.0 s.Figure **S4** (wine curve) shows the WAXS diffractogram of the sample before any photo-thermal experiment. The sample exhibits two wide peaks centered at 8°and 21° which can be attributed to the amorphous structure of the polymer.[1] Further measurements performed on the same sample after some cycles of illumination show identical WAXS patterns, thus confirming that there has been no change in the structure of the P(NIPAm-*co*-NIPMAm) material. It is worth mentioning that the WAXS characterization does not show any peak related to the presence of GNRs because the utilized concentration is under the limit of detection of the instrument.

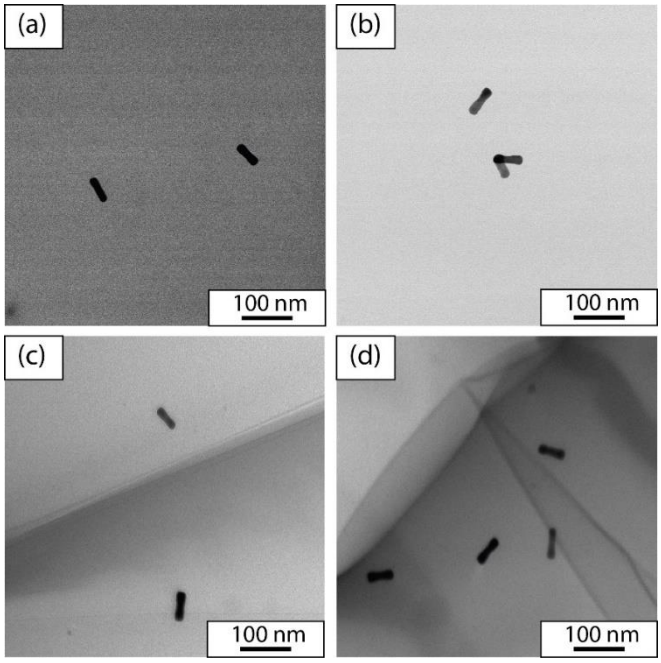

Figure S5. Transmission electron microscope (TEM) analysis of the samples after different cycles of photo-switching experiments: (**a)** - 0 cycles; (**b)** - 1 cycle; (**c)** - 5 cycles; (**d)** - 10 cycles.

Samples were inspected by TEM (see the Experimental Section for technical details) in order to verify if the light-induced thermal heating can produce detectable changes (reshaping) of GNRs. Figure **S5**confirms that even after cycling the samples up to 10 times (Figure **S5-d**), the shape of GNRs turns out to be very similar to the one observed before the photo-switching experiments (Figure **S5-a**). This is a clear evidence that GNRs are stable under the resonant light beam illumination and the reshaping process of GNRs is completely absent.

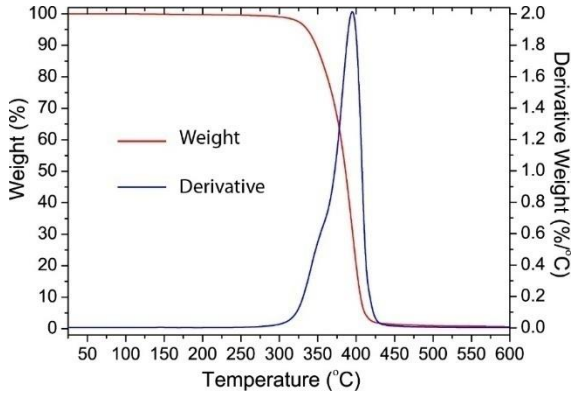

Figure S6. Thermogravimetric analysis of the sample reporting the weight loss (red curve) and its derivative (blue curve).

Lastly, in order to stress out the excellent stability of the P(NIPAm-*co*-NIPMAm)/GNRs samples, a thermogravimetric analysis (TGA) was performed. TGA was carried out by using a TA Instruments SDT Q600 to investigate the thermal stability of the plasmonic hydrogel. The TGA analysis was performed placing around 5.0 mg of sample in an Al_2O_3 pan. The test was carried out by increasing the temperature from 25 °C to 600 °C at a rate of 10 °C/min under a nitrogen flow (100 ml/min) and weighing the sample simultaneously. Figure **S6**shows that the sample is completely stable up to 300 °C. After that point, there is a noticeable weight loss (red curve) which is evidenced by the increasing of its derivative (blue curve).

References

[1]S. Sun, P. Wu, Journal of Materials Chemistry 2011, 21, 4095.

Supporting information2

Thermoplasmonic-activated hydrogel based dynamic light attenuator

*Filippo Pierini, Alexa Guglielmelli, Olga Urbanek, Pawel Nakielski, Luigia Pezzi, Robert Buda, Massimiliano Lanzi, Tomasz A. Kowalewski and Luciano De Sio**

The response function of an ellipsoidal nanoparticle (NP) is related to the extinction cross section through its polarizability tensor α. In the framework of the Gans theory[1], α can be expressed as:

$$\alpha_{||,\perp} = 3\varepsilon_h V_{NR} \frac{\varepsilon_n + \varepsilon_h}{3\varepsilon_h + 3L_{\perp,||}(\varepsilon_n - \varepsilon_h)} \quad (1)$$

where ε_n and ε_h are the dielectric functions of the NP and its surrounding medium, V_{NR} is the NP volume, and:

$$L_{||} = \frac{1-e^2}{e^2}\left(-1 + \frac{1}{2e}\ln\frac{1+e}{1-e}\right) \quad (2)$$

$$L_{\perp} = \frac{1-L_{||}}{2} \quad (3)$$

$$e^2 = 1 - \frac{b^2}{a^2} \quad (4)$$

a and *b* are the long and short axes of the NP, respectively. In order to take into account the real geometry of the NP (in terms of shape and aspect ratio), equation 1 was modified by adding few correction terms[2]. The modified equation for α turns out to be:

$$\alpha_{||,\perp} = 3\varepsilon V_{NR} \frac{\frac{1-0.1(\varepsilon_n+\varepsilon_h)\theta^2}{4}}{\frac{3\varepsilon_h+3L_{\perp,||}(\varepsilon_n-\varepsilon_h)}{\varepsilon_n-\varepsilon_h} + \frac{\Xi_1(0.1\varepsilon_n+\varepsilon_h)\theta^2}{4} + \Xi_2\varepsilon_h^2\theta^4 + \frac{2i\Xi_3\sqrt{\varepsilon_h^3}\theta^3}{3}} \quad (5)$$

where $\theta = 2\pi\omega/c$ (ω is the frequency of the incident radiation and *c* is the speed of light). Equation 5 describes the polarizability tensor for a single NP. It is worth remembering that in the experiments we are in presence of several NPs (randomly oriented). In order to take into

account the presence of several NPs, it is mandatory to utilize the average absorption cross section $\langle C_{abs} \rangle$for a 3D configuration, as reported in[3] . In the actual case, it is possible to simplify the geometry assuming a 2D configuration (NPs are close to the surface). So that, the average absorption cross section can be written as:

$$\langle C_{abs} \rangle = k\Im\left(\frac{1}{2}\alpha_{\perp} + \frac{1}{2}\alpha_{||}\right) \quad (6)$$

where $\alpha_{\perp}, \alpha_{||}$ are the parallel and perpendicular polarizabilities of a single NP and *K* is the wave vector. By implementing a fitting procedure, the obtained parameters are:

$$\Xi_1 = 1.8, \qquad \Xi_2 = 5.5, \qquad \Xi_3 = 2.3 \quad (8)$$

thus, ensuring an excellent agreement with the experimental results reported in Figure 6.

References

[1] R. Gans, Annalen der Physik 1912, 342, 881.
[2] G. Lamri, A. Veltri, J. Aubard, P.-M. Adam, N. Felidj, A.-L. Baudrion, Beilstein Journal of Nanotechnology 2018, 9, 2657.H. Kuwata, H. Tamaru, K. Esumi, K. Miyano, Applied Physics Letters 2003, 83, 4625.
[3] S. B. Singham, C. F. Bohren, Opt. Lett. 1987, 12, 10.